ingegneria sismica
International Journal of Earthquake Engineering
Anno XLIII - Num. 1 - 2026

Research on interference noise elimination and breakdown signal feature extraction technology in GIS voltage withstand field

Lingwen Meng[1,*] *and Fei Gao*[1]

[1] Tongchuan Power Supply Company, State Grid Shaanxi Electric Power Company, Tongchuan 727000, Shaanxi, China

SUMMARY: *In order to realize the wide range of non-contact monitoring and fast and accurate positioning of the voltage breakdown of gas insulated metal-enclosed switchgear (GIS) equipment, and to improve the quality of the installation and commissioning of GIS equipment as well as the progress of the project, the study proposes a non-contact acoustic visualization breakdown positioning technology for GIS equipment. The acoustic sensor array is utilized to collect multi-channel sound signals, extract the abnormal sound image and locate the abnormal sound position. At the same time, a multidimensional filter is designed to filter the noise signal and extract the breakdown signal. Combining the air-domain filtering technology and microphone array signal testing theory, the acoustic visualization algorithm is optimized, the sparse Bayesian solving framework is introduced to accurately solve the unknown source strength, and the diagonal matrix noise reduction is used to suppress the environmental noise and achieve the precise location of the breakdown defects. Experiments show that the frequency band of the breakdown sound signal is about 10Hz~6.7*106Hz, in which the energy attenuation of the audible part is small, which is suitable for non-contact monitoring. Through the improved demodulation scheme, the side-mode rejection ratio is increased by 16.9dB, which effectively improves the accuracy of the detection signal. The system can realize quasi-distributed monitoring with more than 43 probe points, and the positioning accuracy of the middle part of the sensing fiber is up to more than 95%, which effectively reduces the scope of disassembly and overhaul. The research method solves the limitations of traditional ultrasonic localization technology and provides a new technology for efficient fault localization of GIS equipment.*

KEYWORDS: *GIS; voltage withstand; breakdown signal; noise exclusion; localization*

1 Introduction

With the rapid development of science and technology, GIS has gradually become the core equipment of ultra-high-voltage transmission and distribution system by relying on its strong insulating ability, which mainly plays the role of power transmission, distribution and protection [1]. In order to ensure the safe and stable operation and use of GIS, it is necessary to carry out the voltage withstand test, but in the actual test process there is a large amount of interference noise, which seriously affects the accuracy and reliability of the GIS voltage withstand test results [2]. At the same time, GIS is a fully enclosed equipment composed of multiple components and gas chambers, and must be completely disassembled for repair if breakdown occurs during the withstand voltage test, which not only indirectly increases the

*truthtechwx@163.com
https://doi.org/10.65102/is2026015 Published: 30 April, 2026

cost, but also greatly delays the construction progress, so there is an urgent need for a detection method that can quickly determine the location of breakdown faults [3]. Based on this, a large number of scholars at home and abroad have conducted research on it, for example, in order to study the influence of external meteorological factors and internal factors on the occurrence of GIS faults, Zhang Zhaohui's team proposed a support vector machine model, which realized the intelligent diagnosis of the GIS operation status by establishing a nonlinear correspondence [4]. Aiming at the problem that the GIS discharge process is susceptible to noise interference, Yanjun Zhang's team proposed a noise suppression method based on fractional order stochastic autoencoder, which utilizes the autoencoder to perform the conversion of the orthogonal characteristics of the PD signals to achieve the noise suppression, and the results show that the method greatly reduces the interference brought by the external noise [5]. Mudhigollam U K and other scholars have proposed a new thermal network model to accurately analyze the temperature change of the conductor and shell of GIS under different rated currents, the model completes the experimental analysis by insulated switches and current transformers, and it is found that the temperature difference between the conductor and shell of the GIS equipment is 1.2oC~3.3oC under 420kV DC [6]. Facing the difficulty of weak adaptability of traditional discharge diagnosis methods to unlabeled data, Zhang Ruilin et al. proposed a GIS partial discharge diagnosis method based on deformable convolution, which enhances the adaptability to the feature map by virtue of the spatial transformation module, and the study showed that its accuracy of discharge diagnosis was improved by 9.34% on average [7].

At present, although the research on GIS fault identification has made some progress, the traditional methods all have their own limitations. For example, the grounding line current method has shortcomings such as low precision and cumbersome operation in the identification of the discharge breakdown site, while the ultrasonic method, which is more widely used, also has defects such as difficult operation, poor real-time data transmission, and unstable detection results, etc. Therefore, there is an urgent need for a more comprehensive method of locating the GIS voltage-resistant discharge breakdown site [8, 9]. Long Short-Term Memory (LSTM) networks can solve the gradient vanishing and gradient explosion problems existing in traditional recurrent neural networks, and can effectively capture long-distance dependencies in sequences, and have been widely used in long sequence capture scenarios such as language and audio [10]. Therefore, the study takes LSTM as the basic framework for noise exclusion and breakdown signal feature extraction in GIS voltage withstand test site, and introduces Continuous Wavelet Transform (CWT), Recursive Least Squares (RLS), Minimum Variance Distortionless Response (MVDR) algorithms to optimize and improve LSTM to obtain a fusion algorithm. Minimum Variance Distortionless Response (MVDR) algorithms to optimize and improve the LSTM to obtain a fusion algorithm. And combine it with Sparse Bayesian Learning (SBL) based on the Short-Time Fourier Transform (SFTF), Based on this, a non-contact acoustic visualization breakdown positioning technology for GIS equipment was designed, expecting it to solve the problems of poor accuracy, low efficiency and large error existing in traditional positioning methods.

2 Noise exclusion and breakdown signal characterization techniques for GIS equipment

2.1 Classification and Suppression Methods of Multi-source Interference Noise in GIS Pressure Resistant Site

GIS voltage withstand test is an important test method to verify the insulation performance and insulation reliability of GIS, but during the test is susceptible to a variety of noise interference resulting in low accuracy of the test results, a method that can effectively identify the type of noise and inhibit it is needed to ensure the reliability of the results of voltage withstand test [11]. As a special variant of recurrent neural network, LSTM can dynamically adjust the data information and avoid the interference of irrelevant information, which can effectively adapt to the non-stationarity of the GIS voltage withstand field breakdown signal and the strong interference of noise [12]. However, a single LSTM is less efficient in processing complex time series signals, while the extraction ability of the noise signal is limited, and it needs to be optimized.CWT can help to improve the processing efficiency of the algorithmic model on the signal by convolving the wavelet basis function at different scales with the initial signal, and pre-processing the noise while reducing the data dimensions [13]. Therefore, the study introduces the CWT to optimize the LSTM to obtain the Continuous Wavelet Transform and Long Short-Term Memory (CWT-LSTM) hybrid algorithm in order to better extract the noise signal in the discharge breakdown signal, and its specific structure is shown in Figure 1.

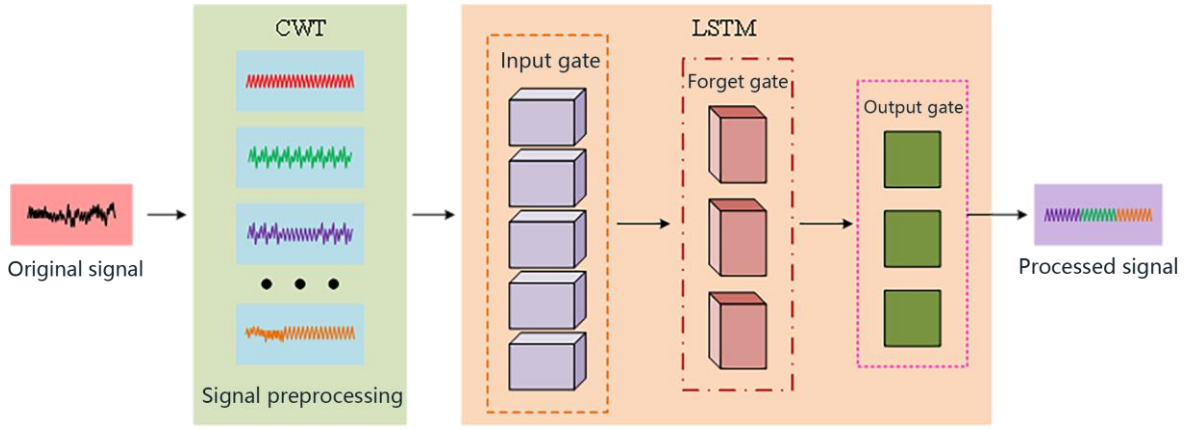

Figure 1: Schematic structure of the CWT-LSTM (pattern source: author's own drawing)

As can be seen from Fig. 1, the hybrid CWT-LSTM algorithm firstly preprocesses the original signal by the CWT, and performs scale scaling and translation operations on the noisy signal through the wavelet basis function to realize the classification of the noisy signal. After that, the preprocessed signal is output to LSTM, and the feature extraction of the signal is accomplished by the three operation units of input gate, oblivion gate, and output gate.The CWT is able to capture the local feature representation of the signal in the time-frequency window, and its functional expression is shown in Equation (1).

$$W_{\phi}(a,b)=[x(t),\phi_{a,b}(t)]=\frac{1}{\sqrt{a}}\int_{-\infty}^{\infty}x(t)\phi(\frac{1-b}{a})dt \tag{1}$$

In Eq. (1), $W_{\phi}(a,b)$ is defined as the process of CWT processing the original signal, $x(t)$ denotes an arbitrary signal including the noise signal at the moment of t, and $\phi_{a,b}(t)$ is the wavelet basis function, which is obtained by the contraction displacement of the mother wavelet function. The specific expression of the mother wavelet function is shown in Eq. (2).

$$\phi_{a,b}(t) = \frac{1}{\sqrt{a}}\phi(\frac{1-b}{a}) \tag{2}$$

In Eq. (2), a represents the scale factor, which is a constant greater than 0, and b is the displacement factor, which takes the value in the range of [0,1], and is used to represent the specific position of the wavelet window in the time domain. And the signal preprocessed by CWT is controlled by the input gate in LSTM to control the degree and quantity of its input, and its specific control process is shown in equation (3).

$$i_t = \sigma(W_i * [h_{t-1}, x_t] + b'_i) \tag{3}$$

In Eq. (3), i_t is the input gate control process, x_t denotes the input signal at the t moment, W_i is the input gate weight, h_t represents the signal output at the t moment, and b'_i is the bias term of the input gate. However, the forgetting gate does not receive all the signals, but filters out the needed signals and forgets the unwanted information, whose function is expressed as shown in equation (4).

$$f_t = \sigma(W_f * [h_{t-1}, x_t] + b'_f) \tag{4}$$

In Eq. (4), f_t represents the forgetting gate screening information, b'_f is the bias term of the forgetting gate, b_f is the weight of the forgetting gate, and σ is the activation function. Although CWT-LSTM can distinguish the noise in the signal, the suppression effect on noise is very limited and needs to be improved. In contrast, RLS, as an adaptive filtering algorithm, minimizes the sum of squares of the errors by recursion, thus dynamically updating the parameters of the algorithmic model, which is suitable for high-precision and fast-convergence scenarios [14]. Therefore, it is studied to improve the CWT-LSTM using RLS to obtain the Recursive Least Squares and Continuous Wavelet Transform and Long Short-Term Memory (RLS-CWT- LSTM) hybrid algorithm to further suppress the noise in the discharge breakdown signal, and its specific structure is shown in Fig. 2.

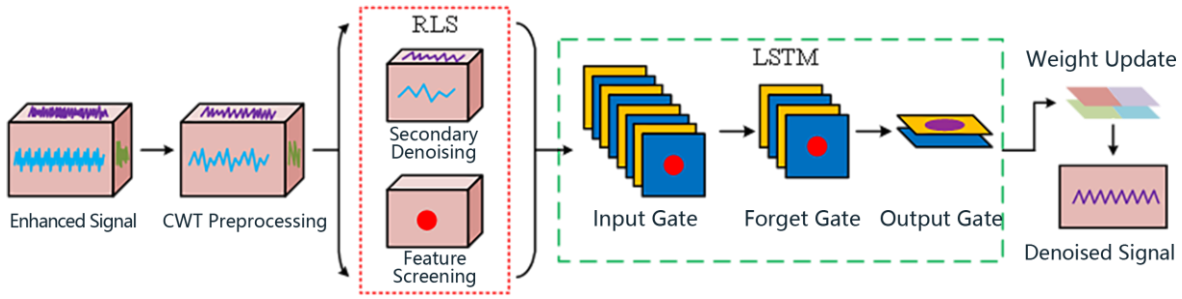

Figure 2: Schematic structure of RLS-CWT-LSTM (pattern source: author's own drawing)

As can be seen from Fig. 2, the optimization of CWT-LSTM by RLS is mainly reflected in

the secondary noise reduction and feature screening of the CWT preprocessing information as well as the weight update of the LSTM output signal. Since the time-frequency feature signals generated by CWT also have redundant signals and irrelevant noise, RLS utilizes a unique recursive mechanism to evaluate the time-frequency components of the feature signals in real time and performs feature component extraction to highlight key signal features. At the same time, the time-frequency component of the noise signal is removed by dynamically adjusting the feature extraction weights of the CWT, thus realizing noise suppression. The specific process in which RLS dynamically updates the feature extraction weights of CWT is shown in equation (5).

$$\theta(n) = \theta(n-1) + \mathrm{K}(n)\left[W'_{clean}(a,b) - \Psi(a,b;\theta(n-1))\right] \tag{5}$$

In Eq. (5), $\theta(n)$ is the feature extraction weight update of the CWT, θ is the parameter vector of the wavelet basis function, $\Psi(a,b;\theta)$ denotes the estimated value of the wavelet transform for the current feature extraction process, $W'_{clean}(a,b)$ is defined as the wavelet coefficients after the quadratic noise reduction, $\mathrm{K}(n)$ is the gain matrix at the nth iteration. In addition, before the LSTM extracts the signal for output, the RLS performs a weight update to improve the quality of the output signal, and the weight update function is expressed as shown in equation (6) [15].

$$w_f(n) = w_f(n-1) + \mathrm{K}(n)\left[f_t^{\text{target}} - \sigma'(w_f(n-1)\cdot h_{t-1} + b'_f) \right] \tag{6}$$

In Eq. (6), $w_f(n)$ is defined as the final wavelet coefficients, σ' is the specific Sigmoid activation function, h_{t-1} denotes the hidden state in the previous moment, and f_t^{target} is the output target of the forgetting gate. However, RLS-CWT-LSTM needs to continue to be optimized for its weak adaptability to the complex dynamic environment and incomplete signal feature extraction when locating the breakdown site in the actual GIS voltage withstand site. MVDR, as an adaptive beamforming algorithm, improves the feature extraction of the target signal by improving the weight vectors of the array antenna or microphone array, while further suppressing the noise to reduce the interference [16]. Therefore, the study introduces MVDR for further optimization of RLS-CWT-LSTM to obtain Minimum Variance Distortionless Response and Recursive Least Squares and Continuous Wavelet Transform and Long Short Term Memory Network (Minimum Variance Distortionless Response and Recursive Least Squares and Continuous Wavelet Transform and Long Short-Term Memory, RLS-CWT-LSTM) fusion algorithm. The fusion algorithm improves the feature extraction capability of the discharge breakdown signal with the help of MVDR, and its specific structure is shown in Fig. 3.

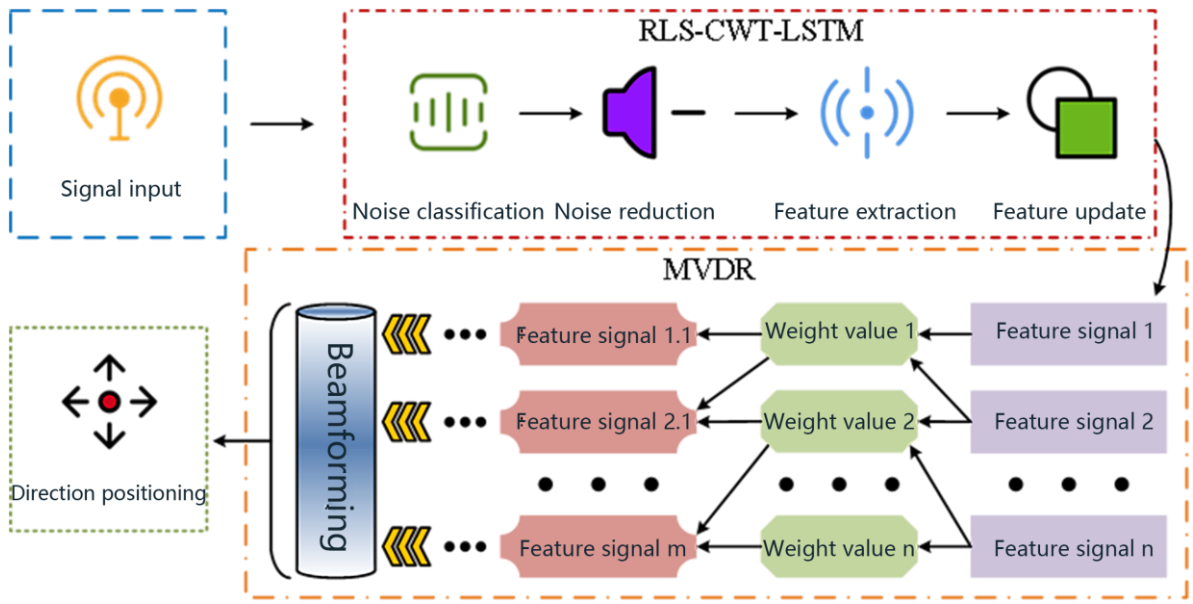

Figure 3: Schematic structure of MVDR-RLS-CWT-LSTM fusion algorithm Pattern (source: https://iconpark.oceanengine.com/home and the author custom painting)

As can be seen in Fig. 3, in the fusion algorithm, MVDR processes the signals output from RLS-CWT-LSTM, and minimizes the response of the algorithm to noise and other interfering signals by adjusting the weights of the signals to achieve the purpose of excluding noise. At the same time, MVDR can also provide a signal distribution space based on beam formation, combining the previously extracted feature signals with it to enrich the feature representation of the discharge signal, which helps to improve the generalization ability of the algorithm. The specific process in which MVDR minimizes the weight output of the interference signal is shown in equation (7).

$$\min_{w} w^{H} R_{w} \quad s.t. \quad w^{H} \tau(\theta') = 1 \tag{7}$$

In Eq. (7), w is the array weighting vector, R is the covariance matrix of the input signal, and $\tau(\theta')$ denotes the orientation vector of the target signal corresponding to the direction θ'.

2.2 Feature extraction technique for breakdown signal based on improved Sagnac interferometer

Although the fusion algorithm is excellent in noise suppression and feature extraction of breakdown signals, it can not deal with strong sparsity signals well, and needs to be combined with related techniques or methods in order to comprehensively extract the discharge breakdown signals.SBL, as a machine learning algorithm based on the Bayesian theory, can be used to recover and reconstruct sparse signals with the help of a priori distributions, and it has a high degree of autonomy and flexibility [17]. Therefore, the study combines it with the fusion algorithm to ensure that the sparsity signal in the breakdown signal can be processed, and its specific structure is shown in Fig. 4.

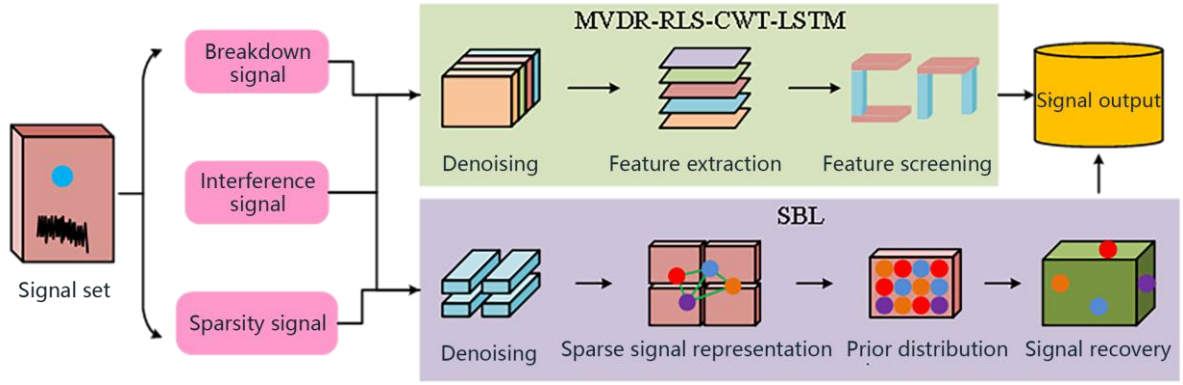

Figure 4: Schematic of the structure of the fusion algorithm combined with SBL (pattern source: author's own drawing)

As can be seen from Fig. 4, the fusion algorithm processes the discharge breakdown signal and the interference signal in the signal collection released from the GIS voltage withstand test site, and completes the feature extraction of the breakdown signal and excludes the interference of the noise through the operations of denoising, feature extraction, and feature screening. On the other hand, SBL is targeted to extract the discharge breakdown signals with sparsity in the signal collection, represent the sparse signals as linear combinations by denoising and sparsity assumption, and then improve the sparsity of the sparse signals by using the hierarchical prior distribution. Finally, the sparse signal is recovered or reconstructed by virtue of Bayesian inference iterative updating, so as to complete the feature extraction of the strongly sparse signal. Where SBL utilizes Bayesian assumptions for sparse signal representation as shown in equation (8).

$$y = \Phi \times \mathrm{s} + \mathrm{n} \tag{8}$$

In Eq. (8), y is defined as the sparse signal representation, Φ is the signal observation matrix, s represents the sparse signal, and n is the interference noise. The SBL, on the other hand, usually relies on the edge likelihood function for iterative updating, which is expressed as shown in Eq. (9) [18].

$$p(y|\alpha, \sigma^{*2}) = \sigma^{*2} \cdot \gamma + \mathrm{s} \cdot \Lambda^{-1} \tag{9}$$

In Eq. (9), p is defined as the evidence function, α is the hyperparameter, σ^{*2} is the noise variance, γ denotes the evidence factor of the hyperparameter, and Λ stands for the diagonal matrix of the hyperparameter, which is used for noise reduction and suppression of environmental noise. And the fusion algorithm will signal output through the output gate of LSTM after extracting the discharge breakdown signal, and its output process is shown in Eq. (10).

$$o_t = \sigma(W_o * [h_{t-1}, x_t] + b'_o) \tag{10}$$

In Eq. (10), b_o and W_o denote the weights of the output gates, which are their bias terms, respectively, and o_t represents the feature signals output by the output gates. However, both SBL and the fusion algorithm are weak in capturing the time-frequency signals of strong non-stationary signals, and SBL is suitable for feature signal extraction of small samples,

which has the risk of overfitting the results and needs to be further improved. While STFT, as a widely used time-frequency analysis method, obtains the time-frequency information of the signal by dividing the signal into multiple segments for Fourier transform, which is suitable for the processing of strongly nonsmooth signals [19, 20]. Therefore, the study uses STFT to optimize and improve SBL to obtain Short-Time Fourier Transform and Sparse Bayesian Learning (SFTF-SBL) hybrid algorithm in order to improve the processing ability of strong non-smooth signals, and its specific structure is shown in Figure 5.

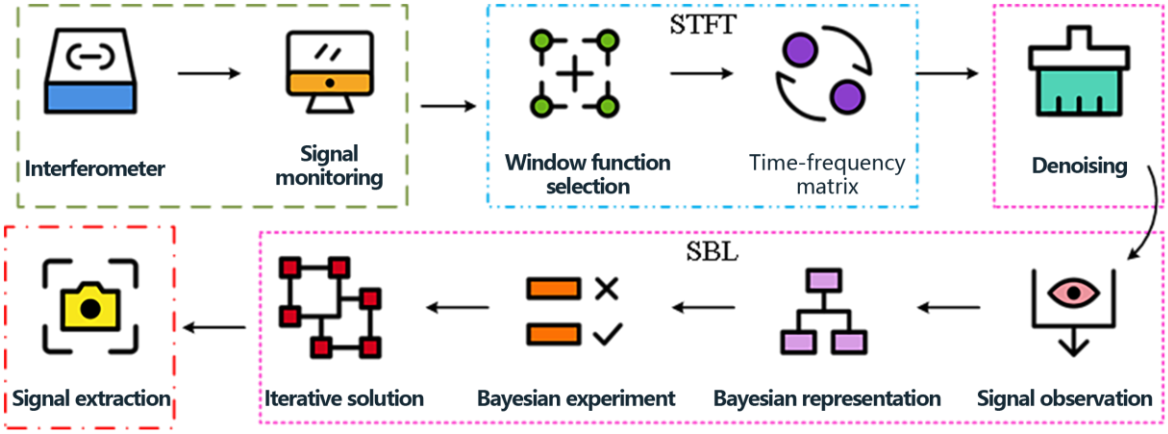

Figure 5: Schematic diagram of STFT-SBL structure (pattern source: https://iconpark.oceanengine.com/home)

As can be seen in Fig. 5, before processing the breakdown signals monitored by the improved Sagnac interferometer, STFT preprocesses the signals, i.e., transforms them into time-frequency matrices by means of suitable window functions and outputs the time-frequency matrices as the results to the SBL, which helps to reduce the dependence on the manual parameter settings of the SBL. After that, SBL relies on a series of operations such as Bayesian representation, prior distribution, and iterative solving to complete the feature extraction of the discharge breakdown signal. In which STFT utilizes the window function for signal time-frequency conversion as shown in equation (11).

$$X(\tau,u)=\int_{-\infty}^{\infty}x^{*}(t^{*})\cdot\omega^{*}(t^{*}-\tau)\cdot e^{-2\pi ut^{*}}\,\mathrm{dt} \tag{11}$$

In Eq. (11), $x^{*}(t^{*})$ is defined as the discharge breakdown signal, $\omega^{*}(t^{*}-\tau)$ is the window function, τ is the time translation parameter used to denote the center of the window function, u represents the frequency parameter, and $X(\tau,u)$ is the STFT time-frequency transformation. In the face of some discrete discharge breakdown signals, the STFT can also be better adapted to the discrete form shown in Eq. (12).

$$X(k^{*},l)=\sum_{r=-\infty}^{\infty}x^{*}\left[m^{*}\right]\cdot\omega^{*}\left[m^{*}-l\right]\cdot e^{-2\pi k^{*}m/N^{*}} \tag{12}$$

In Eq. (12), $x^{*}\left[m^{*}\right]$ denotes the discrete breakdown signals, $\omega^{*}\left[m^{*}\right]$ is a specific certain window function, l is the time window index, k^{*} is defined as the frequency index, N^{*} is the total number of discrete signals. The fusion algorithm has a strong noise suppression capability, and STFT-SBL has a better performance of breakdown signal feature extraction, so the study combines the two to design a new technique for interference noise

exclusion and breakdown signal feature extraction applicable to GIS voltage withstand site, and its specific process is shown in Fig. 6.

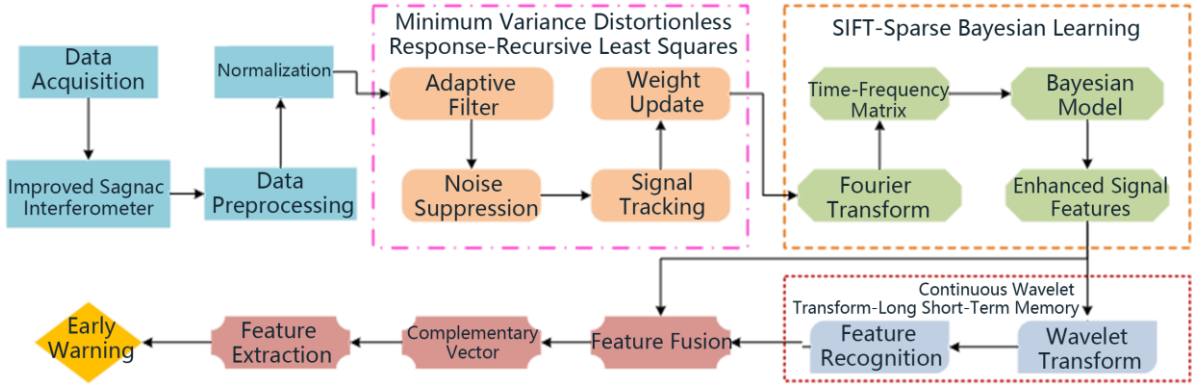

Figure 6: Flowchart of the research technique for processing GIS breakdown signals (Image credit: Author's own drawing)

As can be seen from Fig. 6, the research technique has five main steps in performing the feature extraction of the discharge breakdown signal in the field of GIS withstand voltage test. The first step is to use the improved Sagnac interferometer to monitor the discharge breakdown signals generated by the GIS during the withstand voltage test in an omni-directional real-time manner, and do the pre-processing, including but not limited to data cleaning, de-duplication, and normalization. The second step is to suppress the noise by adaptive filter and rely on RLS to perform the breakdown signal tracking and weight updating operation. The next step is to generate the time-frequency matrix by Fourier transforming the breakdown signal using STFT, and SBL takes the time-frequency matrix as input data to construct a Bayesian model for sparse signal processing, and completes the sparse signal feature extraction through iterative optimization. In the fourth step, CWT performs continuous wavelet transform on the breakdown signal to capture the time-frequency features of the breakdown signal on different scales, and then uses LSTM to predict the temporal dependence of the discharge breakdown signal and extract the signal features. Finally, the sparse signal features and common signal features are fused to complement each other, so as to complete the feature extraction of the discharge breakdown signal of the GIS voltage withstand field and make timely warning.

3 Analysis of experimental results

3.1 GIS breakdown acoustic signal band characteristics and audible sound monitoring analysis

In order to validate the feasibility of the research method, the study compared it with Continuous Wavelet Transform and Multiple Signal Classification (CWT-MUSIC), Improved Convolutional Neural Networks (ICNN) and Finite Impulse Response (FIR) for GIS breakthrough acoustic signal band characterization and audible sound. Convolutional Neural Networks (ICNN) and Finite Impulse Response (FIR) were used to compare the frequency band characterization of GIS penetration acoustic signals with audible acoustic monitoring analysis. The specific experimental environment and experimental parameters were set as follows: Windows 11 Professional, Intel Core i7-14700KF CPU, NVIDIA RTX 5060Ti 16G GPU, Python 3.8 programming language, 64GB DDR5, 6400MHz RAM, 2TB SSD plus 2TB

mechanical hard disk, and 2TB data set. 2TB mechanical hard disk, and the dataset is the COMSOL acoustic module dataset. The dataset is capable of modeling acoustic propagation, reflection and frequency dispersion effects of GIS, while providing frequency band analysis capabilities. The study first compares the accuracy and localization error of four methods for audible sound monitoring, and the experimental results are shown in Figure 7.

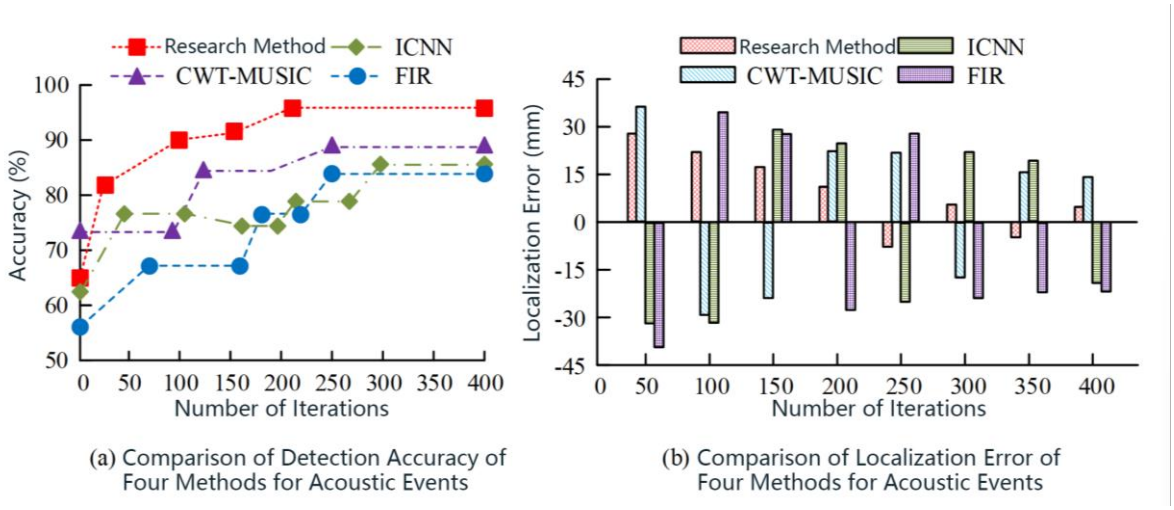

Figure 7: Comparison of the accuracy and localization error of the four methods of audible sound monitoring (Image source: Author's own drawing)

From Fig. 7(a), it can be seen that the maximum accuracy of GIS discharge breakdown audible monitoring using the research method is as high as 96.2%, which is significantly higher than that of 88.4% for CWT-MUSIC, 85.9% for ICNN, and 83.1% for FIR. As can be seen in Fig. 7(b), the localization error of the research method for audible sound monitoring is only 3.6 mm, which is significantly lower than that of CWT-MUSIC (14.8 mm), ICNN (19.4 mm), and FIR (22.5 mm), indicating that the structural design of the localization algorithm in the research method is more reasonable, and it is able to accurately identify the GIS localized discharge breakdown electricity, which is conducive to the reduction of the GIS discharge breakdown identification and Maintenance costs. Then the study of each method for the frequency band characteristics of the breakdown acoustic signal extraction of the time-frequency domain feature parameters to do comparison experiments, the results are shown in Figure 8.

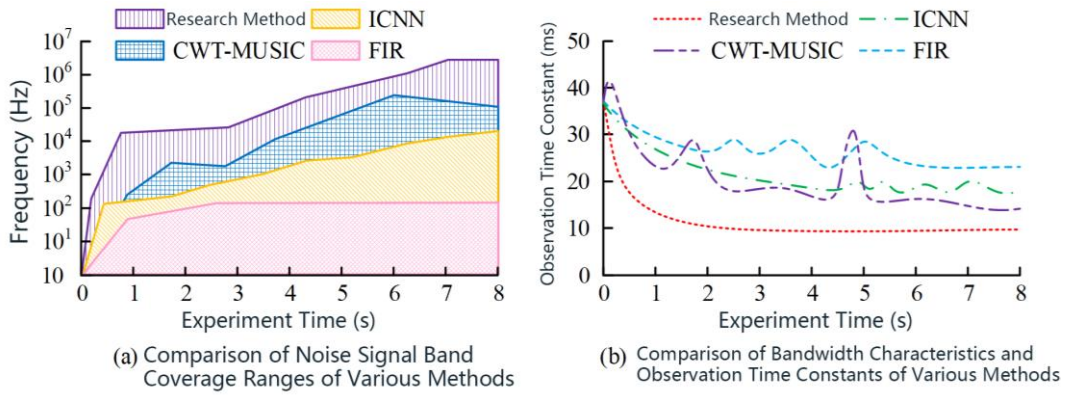

Figure 8: Comparison of feature parameters in time and frequency domain for the extraction of band characteristics of each method (Image source: Author's own drawing)

From Fig. 8(a), it can be seen that the band range of the breakdown acoustic signal extraction by the research method can be up to $6.7*10^6$ Hz, while the band ranges of the CWT-MUSIC, ICNN and FIR breakdown acoustic signals are $3.4*10^5$ Hz, $1.1*10^4$ Hz and $9.6*10^1$ Hz, respectively, and the band ranges are incomplete, which are far inferior to the research method. As can be seen from Fig. 8(b), the decay time constant of band characterization using the research method decreases from 37.6 ms to 9.8 ms, with a difference of 27.8 ms, which is significantly higher than that of CWT-MUSIC (22.3 ms), ICNN (19.7 ms), and FIR (14.9 ms), and the research method can not only accurately locate audible sound when monitoring the band characterization of the GIS penetration signal but also accurately locate audible sound when monitoring the GIS penetration signal. The method not only accurately locates the audible sound with very low error, but also the lower bandwidth and smooth decay time constant indicate that the method is more reliable in monitoring the GIS state.

3.2 Analysis of noise suppression effect of multidimensional filtering and improved demodulation scheme

To further demonstrate the feasibility and superiority of the research method, the study compares it with Convolutional Neural Networks and Support Vector Machine (CNN-SVM), Improved Recursive Least Squares (IRLS) and Improved Orthogonal Matching Pursuit (IOMP) for field test of noise suppression effect. Squares (IRLS) and Improved Orthogonal Matching Pursuit (IOMP) were used to compare the noise suppression effects in the field. The study selects the distribution station of a large factory in Chengdu City, Sichuan Province, as the study area, and the environmentally friendly GIS is used as the study equipment, and the noise suppression ratios and feature retention indices of the four methods are firstly compared experimentally, and the results are shown in Fig. 9.

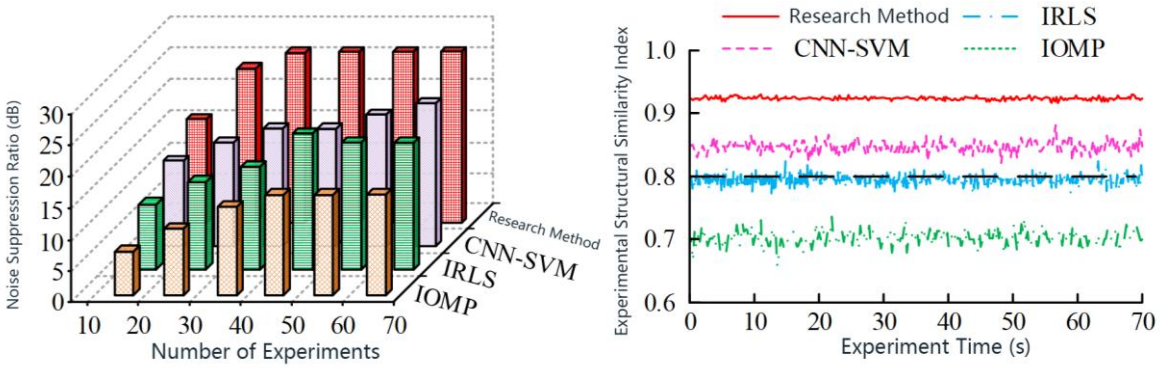

Figure 9: Comparison of noise rejection ratio and feature retention index of the four methods (Image source: Author's own drawing)

As can be seen in Fig. 9(a), the noise suppression ratio of the research method on the breakdown signal is 25.3 dB, which is significantly higher than that of the CNN-SVM method of 18.7 dB, the IRLS method of 15.6 dB, and the IOMP method of 13.1 dB, which indicates that the research method is more capable of suppression of the noise in the breakdown signal, and has a better effect of noise reduction. As can be seen from Fig. 9(b), the average Structural Similarity Index (SSIM) of the signal after noise reduction using the research method is as high as 0.913, which is significantly higher than that of the CNN-SVM method (0.847), the IRLS method (0.798), and the IOMP method (0.706), indicating that the research

method is able to suppress the noise while better retain the key signal features in the original breakdown signal. Next, the computational complexity and processing delay of the noise suppression methods are compared, and the results are shown in Fig. 10.

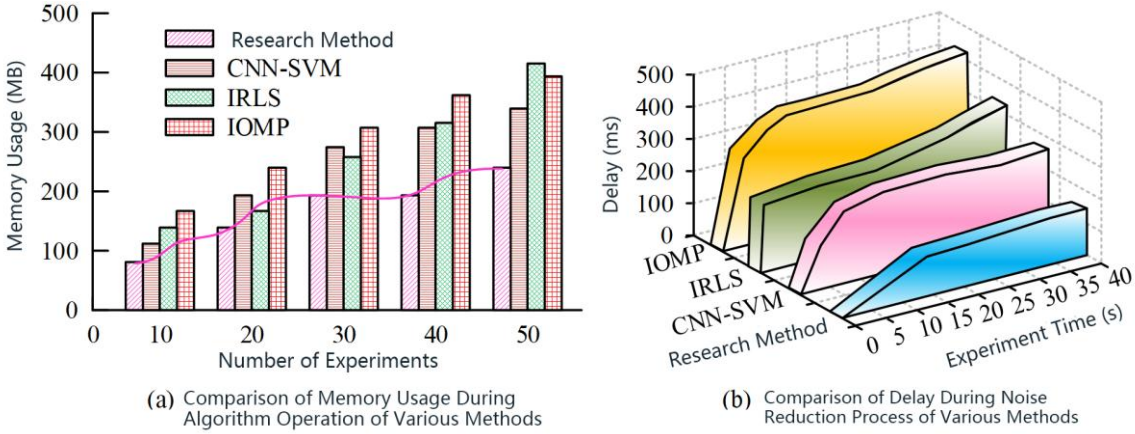

Figure 10: Comparison of the computational complexity and processing delay of the noise reduction process of each method (Image source: Author's own drawing)

From Fig. 10(a), it can be seen that the maximum memory occupancy of the research method in the noise reduction process is as low as 231MB, which is significantly lower than that of CNN-SVM's 318MB, IOMP's 376MB, and IRLS's 402MB, and the tendency of the research method's memory occupancy with the increase of the number of experiments is approximately linear. From Fig. 10(b), it can be seen that the maximum processing delay of the research method is only 158ms, which is significantly lower than that of CNN-SVM's 267ms, IRLS's 326ms, and IOMP's 405ms, suggesting that the research method is more suitable for scenarios requiring real-time monitoring of processed signals. Afterwards, the study compares the false alarm rate of the breakdown signal after noise reduction of different methods, and the experimental results are shown in Table 1.

Table 1: Comparison of false alarm rates of breakdown signals after noise reduction processing by different methods

Type of noise	Number of experiments	False alarm rate of breakdown signal/%			
		Research methodology	CNN-SVM	IRLS	IOMP
Electromagnetic interference noise	10th experiment	0.76	2.03	4.33	5.63
	20th experiment	0.72	2.16	4.62	5.48
	30th experiment	0.68	2.31	4.80	5.31
Machine vibration noise	10th experiment	0.49	1.85	3.94	5.07
	20th experiment	0.57	1.78	3.75	4.78
	30th experiment	0.61	1.70	3.66	4.83
Environmental noise	10th experiment	0.85	2.37	2.73	4.50
	20th experiment	0.81	2.54	2.60	4.34
	30th experiment	0.78	2.49	2.48	4.17

From Table 1, it can be seen that the average false alarm rates of the breakdown signals of the research method after noise reduction for electromagnetic interference, mechanical vibration and three kinds of environmental noises are 0.72%, 0.56% and 0.81%, respectively. The maximum false alarm rate is 0.85%, which is significantly lower than the 2.54% of CNN-SVM, 4.80% of IRLS, and 5.63% of IOMP, indicating that the research method is more

capable of recognizing and removing non-breakdown signals, and is able to effectively avoid misjudging non-breakdown signals as breakdown signals. Finally, the study conducted comparison experiments on the side-mode rejection ratio and the number of quasi-distributed monitoring probe points for the three methods of the research method, CNN-SVM and IRLS, and the results are shown in Fig. 11.

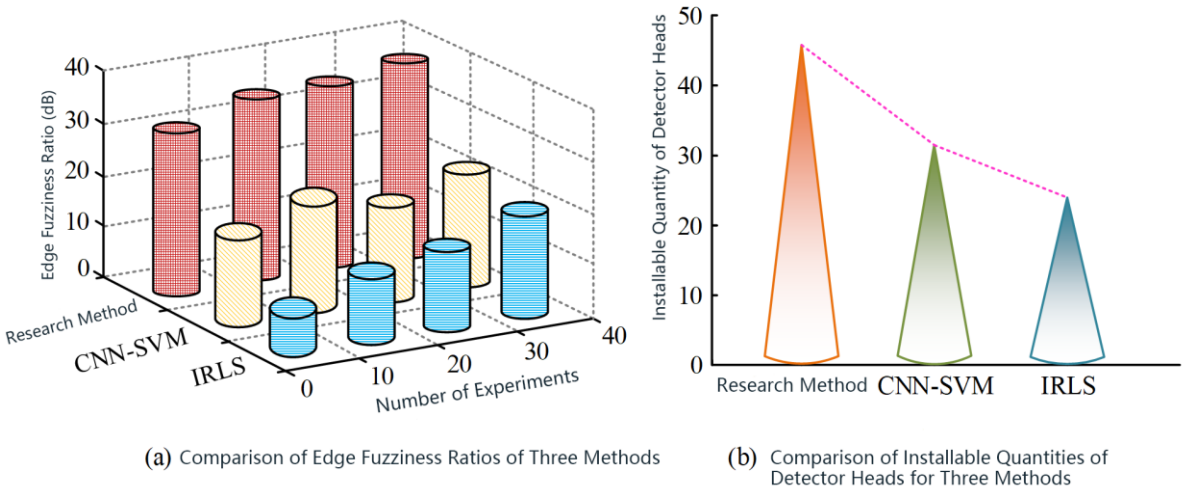

(a) Comparison of Edge Fuzziness Ratios of Three Methods

(b) Comparison of Installable Quantities of Detector Heads for Three Methods

Figure 11: Plot comparing the edge mode rejection ratios of the three methods (Image source: Author's own drawing)

As shown in Fig. 11(a), the maximum side-mode rejection ratio of the research method is 35.3 dB, which is significantly higher than that of CNN-SVM (20.2 dB) as well as that of IRLS (18.4 dB), and the side-mode rejection ratio of the improved research method is improved by 16.9 dB compared with that of IRLS, which indicates that the main-mode power of the laser signal transmitter is higher than the side-mode and the signal quality is better. From Fig. 11(b), it can be seen that 46 quasi-distributed monitoring probe points can be installed when utilizing the research method for noise suppression at the GIS withstand site, which is much higher than the 31 of the CNN-SVM and the 23 of the IRLS, and helps to improve the accuracy of the breakdown signal monitoring. In summary, the research method possesses strong multi-dimensional noise suppression capability and high-precision feature extraction of breakdown signals, and at the same time can timely and accurately locate the GIS discharge breakdown site.

4 Conclusion

Aiming at the low accuracy and poor efficiency of the current GIS voltage withstand field discharge breakdown signal feature recognition methods, the study proposes a non-contact acoustic visualization breakdown localization method for GIS equipment based on MVDR-RLS-CWT-LSTM with STFT-SBL, and proves its feasibility through comparative experiments. The results show that the noise suppression by this technique has a noise rejection ratio of 25.3 dB, an average SSIM value as high as 0.913, the memory occupation and processing delay of the noise reduction process are 231 MB and 158 ms, respectively, and the maximum side-mode rejection ratio is 35.3 dB. And in the feature extraction experiment of the breakdown signals, the research method monitors the audible sound with an accuracy as high as 96.2%, and the audible sound In the feature extraction experiment, the accuracy of the research method in monitoring the audible sound is as high as 96.2%, and the localization

error of the audible sound is as low as 3.6mm, the maximum frequency band range is from 10Hz to $6.7*10^6$Hz, and the decay time exponent is 9.8ms. Meanwhile, the maximum false alarm rate of the piercing signal after the noise reduction process is 0.85%, and the number of quasi-distributed monitoring probes that can be mounted is as high as 46 points. The above experimental data are better than the comparison method, which fully proves the feasibility and superiority of the research method, and provides a new method for exploring the noise exclusion and breakdown signal characterization of GIS voltage withstand site. Although the actual performance of the research method is good enough, the comparison experiment does not differentiate the experimental environment, and only one environment is selected for the GIS voltage withstand test site, so it should be the focus of further research in the subsequent study.

Funding

Scientific and Technological Project of State Grid Shaanxi Electric Power Company: Research on Acoustic Visualization-Based Defect Localization and Diagnosis Technology for GIS Equipment Using Spatio-Temporal Feature Fusion.

References

[1] ZHU Youkun, WANG Qinwei, WANG Yuangang, et al. Research on laser sealing welding process of gas insulated switchgear filling box[J]. Laser Journal, 2024, 45(10):236-239.

[2] HUANG Tao, SUN Hengdong, JIANG Jun, et al. Application of fiber-optic distributed acoustic sensing system in GIS voltage withstand test[J]. Laser Technology, 2023, 47(4):459-462.

[3] Luo Y, Mao S, Tang J, Pan Z, Pan C. Shape optimisation of basin insulator for DC gas insulated switchgear/gas insulated transmission lines based on artificial bee colony algorithm[J]. High Voltage, 2024, 9(2): 275-286.

[4] ZHANG Zhaohui, ZHAO Ke, CHEN Shaobo, et al. Research on operation feature extraction and fault diagnosis technology of gas-insulated switchgear[J]. Manufacturing Automation, 2024, 46(6):132-138.

[5] ZHANG Yanjun, XU Su, ZHANG Ruiqiang, et al. Partial discharge noise suppression method for GIS equipment based on F-SAE network[J]. New technology of electric power and electric energy, 2025, 44(1):118-128.

[6] Mudhigollam U K, Tiwari N, Rao M M. Transient thermal analysis of gas insulated switchgear modules using thermal network approach[J]. International Journal of Emerging Electric Power Systems, 2024, 25(2): 163-174.

[7] ZHANG Ruilin, ZHANG Yue, SUN Xiaolan, et al. A diagnosis method of GIS partial discharge based on deformable convolution and self-supervised comparative learning[J]. High Voltage Technology, 2024, 50(11):5022-5033.

[8] YAN Zeyu, YANG Yang, LIU Yunpeng, et al. Multi-perception GIS partial discharge

identification based on neurally supervised decision tree algorithm[J]. Chinese Journal of Electrical Engineering, 2024, 44(14):5821-5832.

[9] JIANG Zhisong,ZHANG Baoqing,LI Xiaolong,et al. Automatic detection algorithm for GIS equipment based on WSN and ultrasonic vibration signal recognition[J]. Microcomputer Applications, 2024, 40(11):83-86.

[10] LI Haolei, ZHAO Sheng, XIE Xilong, et al. Research on lithium battery charge state estimation based on GWO-LSTM-TCN hybrid model[J]. Power Supply Technology, 2024,48(11):2195-2200.

[11] Du S, Cheng X, Ge G, Li T, Guo L, Liu S. AC breakdown and decomposition products detection characteristics of eco-friendly insulating medium in gas insulated switchgear[J]. Scientific Reports, 2024, 14(1): 19491-19502.

[12] FAN Lei, ZHANG Qian, LI Guoli, et al. Short-term photovoltaic power generation prediction based on digital twins of long and short-term memory networks[J]. Modern Electric Power, 2023, 40(6):899-905.

[13] HU Congqiang, QU Na, ZHANG Shuai, et al. Application of continuous wavelet transform and deep residual contraction network with attention mechanism in low voltage series arc fault detection[J]. Grid Technology, 2023, 47(5):1897-1904.

[14] LIN Shunfu, LI Yukun, CHENG Weijian, et al. An improved recursive least squares method for system harmonic impedance estimation[J]. Grid Technology, 2023, 47(7):2879-2886.

[15] ZHU Minghui, GU Peng, GAO Dong. A recursive least squares based differential measurement and estimation method of remanent magnetization for moving platforms[J]. Journal of Space Science, 2024, 44(3):570-584.

[16] WANG Tianqi, YANG Xiangguo, YAN Yuan, et al. A gas leakage localization method based on improved minimum variance distortion-free response angle spectrum algorithm[J]. Applied Acoustics, 2024, 43(1):110-118.

[17] Mu Xinru, Fu Haijun, Dai Jisheng. Sparse Bayesian learning based boda direction estimation for hybrid mMIMO systems[J]. Data Acquisition and Processing, 2024, 39(5):1260-1270.

[18] TAN Yufan, FENG Haihong, LI Jilong, et al. A time-domain channel parameter estimation method based on improved sparse Bayesian learning[J]. Acoustic Technology, 2024, 43(6):896-906.

[19] ZHU Qinyue, YU Yichen, ZHAN Yanwen, et al. Modular multilevel converter submodule IGBT open-circuit fault diagnosis based on short-time Fourier transform and deep network[J]. Journal of Electrotechnology, 2024, 39(12):3840-3854.

[20] ZHENG Dezhi, QIAO Mengtian, LI Zhongxiang, et al. Research on array-based sensor intrusion signal acquisition and layer counting algorithm[J]. Journal of Instrumentation, 2023, 44(3):221-233.